The Astrophysical Journal Supplement Series, 193:26 (10pp), 2011 April doi:10.1088/0067-0049/193/2/26

THE M 33 SYNOPTIC STELLAR SURVEY. I. CEPHEID VARIABLES

Anne Pellerin and Lucas M. Macri[1]
George P. and Cynthia Woods Mitchell Institute for Fundamental Physics and Astronomy,
Department of Physics and Astronomy, Texas A&M University, 4242 TAMU, College Station, TX 77843, USA;
pellerin@physics.tamu.edu, lmacri@physics.tamu.edu
Received 2010 December 17; accepted 2011 February 8; published 2011 March 14

ABSTRACT

We have conducted a ground-based *BVI* synoptic survey of the Local Group galaxy M 33 which covers most of its disk and spans a period of 7 years. The survey targets luminous, long-period variables such as Cepheids and Miras and combines images from the DIRECT project and follow-up observations at the WIYN 3.5 m telescope. This paper, the first in a series, presents the discovery and characterization of 564 Cepheid variables, which represent a factor of two increase over previous samples with calibrated point-spread function (PSF) photometry. We also describe the details of the observations and analysis of the survey data, including the use of archival *Hubble Space Telescope* images to characterize biases in our ground-based PSF photometry.

Key words: galaxies: individual (M 33) – stars: variables: Cepheids

Online-only material: color figures, machine-readable tables

1. INTRODUCTION

The study of Cepheid variables in nearby galaxies has been a very active field for nearly 100 years (Leavitt & Pickering 1912), due to the crucial role they played in establishing the extragalactic nature of "spiral nebulae" (Hubble 1925) and later in the determination of the Hubble constant, H_0. Over the past two decades, observations of Cepheids with the *Hubble Space Telescope* (*HST*) have resulted in a significant improvement on the accuracy and precision in the determination of H_0. The first generation of *Hubble* projects aimed at measuring H_0 had uncertainties of ∼10% (Freedman et al. 2001; Sandage et al. 2006), while more recent work has reduced that to 5% (Riess et al. 2009). The accuracy and precision in the measurement of the Hubble constant via Cepheid variables and secondary distance indicators has a direct impact on the constraints in the equation of state of dark energy (Komatsu et al. 2011). Thus, improving our understanding of the properties of Cepheid variables remains an important and active area of observational and theoretical research.

M 33 has been the target of numerous surveys for Cepheids and other variable stars, starting with Hubble (1926), due to its relative proximity and its moderate inclination angle. The DIRECT survey (Stanek et al. 1998) carried out the first large-area CCD-based synoptic survey of M 31 and M 33 with the aim of discovering detached eclipsing binaries and Cepheid variables. Results for the central region of M 33 were presented by Macri et al. (2001b) who published calibrated point-spread function (PSF) photometry for 251 Cepheids. Follow-up observations by Mochejska et al. (2001a, 2001b), analyzed via difference-imaging photometry, yielded additional short-period Cepheids. More recently, Hartman et al. (2006) carried out a survey of the entire disk of M 33 and identified ∼2500 Cepheid candidates via difference imaging, although the photometric calibration of this sample is still pending.

Among the many eclipsing binaries discovered by DIRECT in M 33 there are at least two detached systems well suited for distance determination. Bonanos et al. (2006) analyzed one of these systems and derived a distance of 964 ± 54 kpc, equivalent to a distance modulus $\mu_0 = 24.92 \pm 0.12$ mag. However, their results are somewhat at odds (2.7σ discrepancy) with previous Cepheid-based distance moduli for M33: 24.65 ± 0.12 mag (Macri 2001), 24.62 ± 0.08 mag (Freedman et al. 2001), and 24.53 ± 0.11 mag (Scowcroft et al. 2009). The analysis of additional detached eclipsing binary systems in M33 will hopefully resolve this discrepancy and further reduce the uncertainty in its distance. M33 would then become an important contributor to the "first rung" of the Extragalactic Distance Scale, provided its Cepheid sample is properly calibrated. This was one of the main motivations for our survey. An additional motivation for studying the Cepheids in M 33 was the steep abundance gradient measured across its disk by Zaritsky et al. (1994) and Magrini et al. (2007), which would enable a robust determination of the "metallicity dependence" of the Cepheid distance scale. However, Bresolin et al. (2010) and Bresolin (2011) recently presented evidence for a shallow abundance gradient in the disk of M 33, with a mean value very similar to the Large Magellanic Cloud (LMC).

The relative proximity of M 33 minimizes the impact of unresolved blends and crowding in PSF photometry, which can lead to an overestimation of Cepheid magnitudes and biases in their measured colors. Both effects must be properly taken into account in any study of Cepheid variables, since they can contribute to an underestimation of the host galaxy distance. Extensive work must be performed to properly quantify these effects. In the case of nearby ($D \lesssim 2$ Mpc) galaxies, archival *HST* images can greatly help with this task, as shown by Mochejska et al. (2000, 2001c) and Bresolin et al. (2005).

This paper presents the discovery and characterization of a sample of 564 Cepheids in M 33 resulting from a ground-based *BVI* synoptic survey which covers most of the disk of M 33 and spans a period of 7 years. We describe our survey in Section 2 and discuss the details of the photometry and Cepheid light curve fitting in Section 3. Color–magnitude diagrams (CMDs) and Cepheid period–luminosity (PL) relations are presented in Section 4. We address the issue of stellar crowding and

[1] Visiting Astronomer, Kitt Peak National Observatory, National Optical Astronomy Observatory, which is operated by the Association of Universities for Research in Astronomy, Inc. (AURA) under cooperative agreement with the National Science Foundation. The WIYN Observatory is a joint facility of the University of Wisconsin-Madison, Indiana University, Yale University, and the National Optical Astronomy Observatory.

our method for characterizing this effect using archival *HST* images in Section 5. We present our catalog in Section 6 before concluding.

2. OBSERVATIONS OF M 33

This survey combines the data obtained by the DIRECT project with follow-up observations obtained at the Wisconsin–Indiana–Yale–NOAO (WIYN) Observatory. The observations span a minimum of 7 years (up to 10 years for a few fields). In this section, we describe the two data sets in detail.

2.1. Images from the DIRECT Project

As part of an effort to improve the absolute calibration of the Extragalactic Distance Scale, the DIRECT project[2] obtained *BVI* observations of M 33 over ∼200 nights between 1996 September and 1999 November. Most of the survey was carried out at the F. L. Whipple Observatory (FLWO) 1.2 m telescope on Mount Hopkins, Arizona, with additional images obtained at the Michigan–Dartmouth–MIT 1.3 m telescope on Kitt Peak, Arizona. The project observed 11 different fields, each $11\farcm5 \times 11\farcm5$ in size, which covered most of the M 33 disk (see Figure 1). Most of the DIRECT observations were obtained in the *V* band, which provided sensitivity to both early-type detached eclipsing binaries and Cepheid variables. The typical seeing at the FLWO telescope was $\sim 1\farcs5$, and the three different cameras used by the project had pixel scales of $\sim 0\farcs32\,\mathrm{pixel}^{-1}$. Exposure times were 1200, 900, and 600 s per image in the *B*, *V*, and *I* bands, respectively. A more detailed description of the DIRECT observations of M 33 can be found in Macri et al. (2001a, 2001b). The latter publication presented the discovery of 251 Cepheids and additional variables in the three central DIRECT fields within M 33.

2.2. Images from WIYN

While the images obtained by the DIRECT project provided an excellent synoptic data set for the discovery of Cepheids and eclipsing binaries, they were less than ideal for a proper characterization of the photometric properties of these variables. The DIRECT project focused on delivering the best possible phase coverage for the variables, and therefore spent very little telescope time observing standard star fields. This made it difficult to obtain a very accurate photometric calibration. Additionally, the relatively poor seeing at the FLWO 1.2 m made the DIRECT light curves more susceptible to blending and crowding biases. To remedy these issues and further extend the temporal baseline offered by the DIRECT project, we collected additional images at the WIYN 3.5 m telescope between 2002 August and 2006 December. We used the Mini-Mosaic imager, which consists of two CCDs of 4096 × 2048 pixel^2 each, separated by a small gap. The native pixel scale of the camera is $0\farcs14\,\mathrm{pixel}^{-1}$, leading to a field of view of $9\farcm6 \times 9\farcm6$. Eighteen separate pointings were required to cover the same area as the DIRECT project. Each pointing was offset in declination by about half the field of view, relative to the preceding pointing. This observing strategy led to 29 different fields of $9\farcm6 \times 4\farcm8$ each (see Figure 1), with slight overlaps in both directions. The images were binned by a factor of two to reduce the readout time, leading to an effective sampling of $0\farcs28\,\mathrm{pixel}^{-1}$. Exposure times were 90 s in *B*, 60 or 90 s in *V*, and 30 or 60 s in *I*, to match the depth of the DIRECT images. A detailed observation log for the WIYN data is presented in Table 1. The 29 WIYN fields are identified from 0 to 9 and *a* to *s*, as labeled in Figure 1.

Table 1
WIYN Observation Log

Date	MJD (days)	Field	Band	Exp. Time (sec)	Seeing (arcsec)
2002 Aug 12	2499.40241	*c*	*I*	30	1.57
2002 Aug 12	2499.40241	*d*	*I*	30	1.55
2002 Aug 12	2499.40552	*d*	*V*	60	2.12
2002 Aug 12	2499.40552	*c*	*V*	60	1.85
2002 Aug 12	2499.40749	*d*	*B*	90	1.65
2002 Aug 12	2499.40749	*c*	*B*	90	2.01
2002 Aug 12	2499.41333	*c*	*I*	30	0.69
2002 Aug 12	2499.41333	*b*	*I*	30	0.60
2002 Aug 12	2499.41571	*b*	*V*	60	0.71
2002 Aug 12	2499.41571	*c*	*V*	60	0.83

(This table is available in its entirety in a machine-readable form in the online journal. A portion is shown here for guidance regarding its form and content.)

3. DATA REDUCTION AND ANALYSIS

All images were subject to overscan correction, bias subtraction, and flat fielding using the MSCRED package in IRAF.[3] Given the high density of stars in our images, particularly in the central part of M 33, we performed PSF photometry using the DAOPHOT, ALLSTAR, and ALLFRAME (Stetson 1987, 1994) programs. Due to the large number of images in our data set, we used a series of Tcl/Tk-based scripts originally developed by the DIRECT project to run these programs in batch mode. A detailed description of the individual steps that were performed is presented below.

3.1. PSF Photometry

We performed PSF photometry on every individual image as follows. We used the DAOPHOT task FIND to identify point-like sources 5σ above background and obtained magnitudes through a 7 pixel (∼2.1) radius aperture using PHOT. We used PICK to obtain a list of 200 bright, isolated stars that might be suitable to determine the PSF. Due to the high stellar density of our fields, the list of stars returned by this task contained a large fraction of blended or crowded objects. Given the large number of images we had to process, it was not practical to remove these unsuitable stars by hand as it is often done, nor to rely on an iterative application of the DAOPHOT PSF task. Instead, we developed an IDL-based routine that fit a two-dimensional Gaussian profile to every star in the initial list of PSF stars. We rejected objects whose full width at half-maximum (FWHM) values in either the *x*- or *y*-axis were more than 1σ from the median, as well as any objects whose ellipticity was larger than 3σ from the median. This removed elongated sources that could be two or more stars as well as background sources such as galaxies. We also calculated the residuals from the Gaussian fit and eliminated sources with residuals that were 3σ or greater than the median value. This removed sources located in very crowded regions. We kept a minimum of 25 stars in order to create a reliable PSF model, increasing the initial sample returned by PICK if necessary. Once we obtained the desired sample of bright and

[2] http://www.astronomy.ohio-state.edu/∼kstanek/CfA/DIRECT/

[3] IRAF is distributed by the National Optical Astronomy Observatory, which is operated by the Association of Universities for Research in Astronomy (AURA) under cooperative agreement with the National Science Foundation.

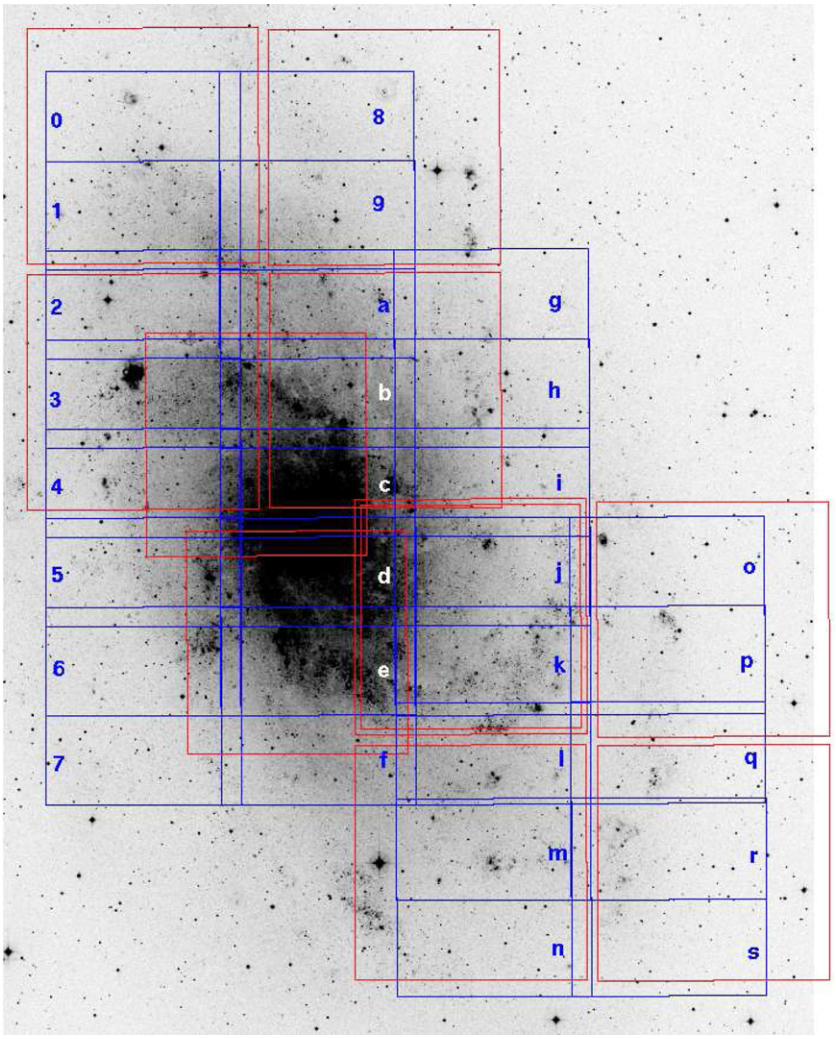

Figure 1. Digitized Sky Survey image of M 33 showing the location of the DIRECT fields (red) and our follow-up WIYN observations (blue). The image is about $40' \times 50'$ in size. The WIYN fields are also labeled in blue or white. North is up and east is to the left.
(A color version of this figure is available in the online journal.)

isolated stars, we ran the PSF task iteratively with the ALLSTAR program as prescribed in the DAOPHOT manual. Typical PSF FWHM values were 0.″7 and 1.″5 for the WIYN and DIRECT images, respectively. Once all model PSFs had been determined, we performed PSF photometry on every star in every frame using ALLSTAR.

We created master images for each of the 29 fields in each of the three bands, derived frame-to-frame transformations, and carried out the final PSF photometry as follows. We selected 4–7 images from the WIYN observations, with the smallest FWHM and low sky values, to make the master image. We used the DAOMATCH and DAOMASTER programs to derive the positional transformations between these images and combined them using the MONTAGE program. We performed PSF photometry as described above to obtain a master star list, which we matched to the star list of every frame using DAOMATCH and DAOMASTER to derive frame-to-frame transformations. Next, we ran ALLFRAME using the master star list and the derived transformations to obtain consistent PSF photometry for all stars in all images of a given field and filter. We will refer to these measurements as "WIYN+DIRECT photometry." We performed artificial star tests on the master frames and derived a 90% completeness limit at typical magnitudes of 23.3, 23.1, and 21.5 mag in the *B*, *V*, and *I* bands, respectively. These completeness limits change slightly from field to field depending on the stellar density.

After we carried out the previous analysis, we found that the DIRECT images have significant distortion in their corners, which in a few cases was beyond the ability of DAOMASTER and ALLFRAME to compensate for. This seriously degraded the quality of light curves in small regions within our survey area. Hence, we created a second set of master images based only on DIRECT data and performed a separate round of ALLFRAME photometry on DIRECT images only. We will refer to these measurements as "DIRECT-only photometry." This allowed us to obtain good light curves at the corners of the DIRECT fields, at the price of brighter limiting magnitudes and higher risk of stellar blends. In order to mitigate these effects, we performed a third round of ALLFRAME photometry on the WIYN images only (hereafter the "WIYN-only photometry"), based on the original WIYN-based master frames described above. We matched the stars between the DIRECT-only and WIYN-only sets and used the light curves from the latter set in our final analysis. This will be discussed in more detail in Section 3.2. Note however that, as shown in Figure 1, some DIRECT fields extend to areas not covered by the WIYN fields. Consequently, the DIRECT-only

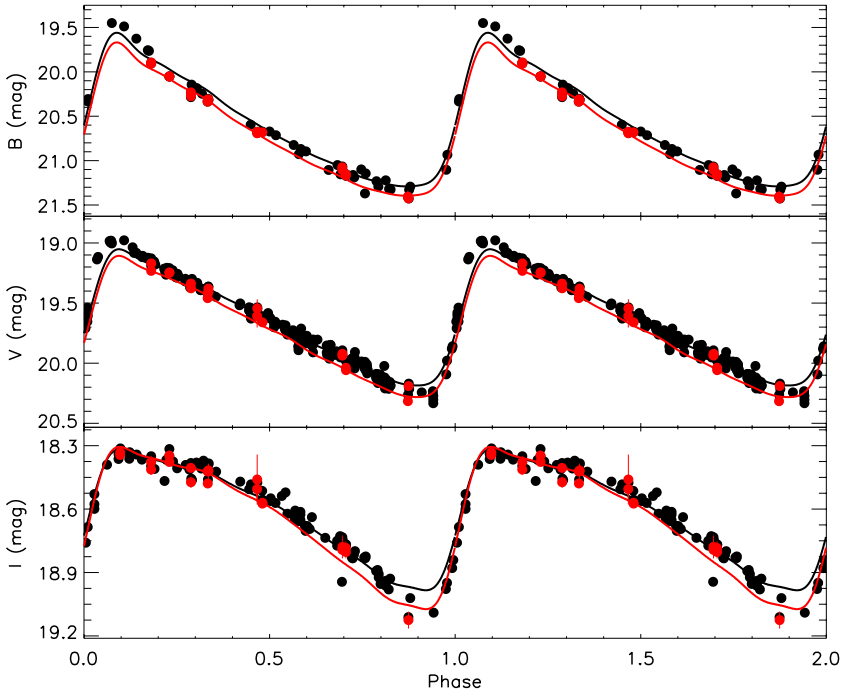

Figure 2. Example of *BVI* light curves for one of the Cepheids in our sample (J013302.0+303634.3, $P = 30.501$ days) illustrating the different sampling provided by the WIYN+DIRECT and WIYN-only observations (black and red symbols, respectively). The black and red lines indicate the best-fit template light curves for the combined and WIYN-only photometry, respectively. Photometric uncertainties are only plotted for the WIYN observations to ensure clarity.

(A color version of this figure is available in the online journal.)

photometry gave us an additional ∼170 arcmin^2 area for the Cepheid search, which can be visualized in Figure 1.

3.2. Variable Search, Period Determination, and Light Curve Fitting

We identified variable stars and extracted their light curves using the TRIAL program (Stetson 1996). This program derived final frame-to-frame photometric offsets using a list of bright, isolated, and constant-magnitude stars, which we selected based on the ALLFRAME output, and calculated a variability index J for each star. We extracted light curves for all sources displaying $J > 0.75$ and searched for periodicity using an IDL implementation of the CLEAN algorithm[4] (Högbom 1974; Roberts et al. 1987). We selected up to eight trial periods that were at least 10σ above the noise level of the periodogram. We simultaneously fit the phased *BVI* light curves using the Cepheid templates of Yoachim et al. (2009) and selected the trial period that returned the lowest χ^2 value for further inspection. The *B*-band templates were kindly provided to us by P. Yoachim (2009, private communication), since they were not part of their original work. The fit returned mean magnitudes and light curve amplitudes for each band. We did not constrain the light curve amplitudes to obey the "canonical" 1.4:1:0.7 *BVI* ratios, since we planned to use the observed amplitude ratios to identify possible blends as described below. The *V* and *I* light curves are usually better fitted by the templates than the *B*-band data because the latter contain a significantly lower number of epochs. This leads to slightly larger uncertainties in the mean magnitude and amplitude values in *B*.

We gave preference to the "WIYN+DIRECT" photometry for the variability and period search, except for the regions that were affected by the optical distortion described in Section 3.1 where we used the "DIRECT-only" light curves. There are 153 out of 667 stars for which the variability and period search was based on "DIRECT-only" images. The final magnitudes and pulsation amplitudes we report are based on light curve template fits to the "WIYN-only" photometry, to minimize the effects of blending and crowding. Figure 2 shows a comparison of the light curves for one Cepheid derived from the "WIYN+DIRECT" and "WIYN-only" observations. The former tends to have flatter minima and slightly reduced amplitudes, which are signs of blending in the DIRECT data.

In a few cases where the WIYN coverage was too sparse or non-existent, we were forced to use "DIRECT-only" light curves; these exceptions are properly identified in our final catalogs. Thirty-six variables have no WIYN image counterpart, hence have DIRECT-only light curves.

3.3. Astrometric and Photometric Calibration

We based our astrometric and photometric calibrations on the stellar catalog of M 33 published by Massey et al. (2006). We carried out the astrometric calibration using the WCSTools package.[5] We used the initial WCS provided by the telescope control system to identify bright stars in common between the master frame of each field and filter and the reference catalog. We constructed a paired list of master frame (x, y) positions and Massey et al. celestial coordinates and used the imwcs task to determine the astrometric solution. We used eight parameters for the astrometric solutions, with the exception of a few outer fields where the lower stellar density did not yield a sufficient number of bright stars in common. In those cases, we carried out a six parameter fit. The typical astrometric residuals were less than $0\farcs2$.

[4] http://www.arm.ac.uk/~csj/idl/CLEAN/clean.pro

[5] http://tdc-www.harvard.edu/software/wcstools.html

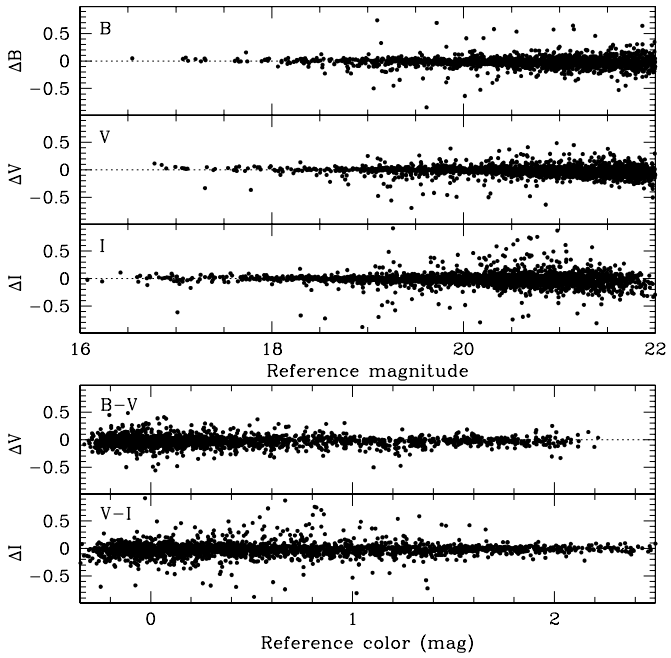

Figure 3. Comparison of photometry between our final calibrated catalog and the reference catalog of Massey et al. (2006) for one of the 29 fields in our survey, located at an intermediate galactocentric radius. The top three panels show the magnitude differences in B, V, and I as a function of the reference catalog magnitudes in the respective band. The bottom two panels present the difference in V and I as a function of $B-V$ or $V-I$ color of the reference catalog, respectively. In all panels, the comparison was restricted to stars with three-band photometry, a low variability index ($J < 0.75$), and photometric errors below 0.05 mag.

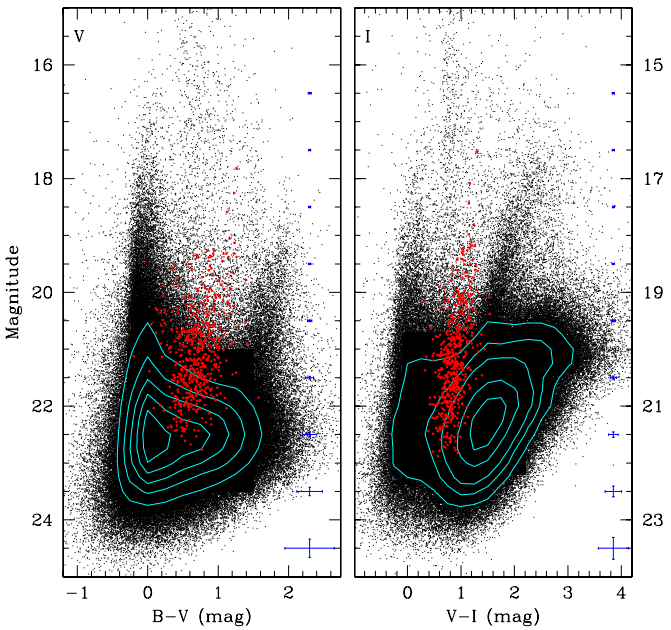

Figure 4. Color–magnitude diagrams of all stars detected by our survey. Small black points: all stars detected in the WIYN master images. Filled red symbols: Cepheid variables. Green contours show the stellar density in the saturated regions of the diagrams. The median photometric uncertainties in magnitude and color for each bin are indicated by blue error bars on the right of each diagram.

(A color version of this figure is available in the online journal.)

Once we had established a common WCS between our catalog and Massey et al., we expanded our search to select common stars that could be used to derive the photometric calibration of our instrumental magnitudes. We derived photometric zero points and color terms based on stars detected in all three bands in both catalogs, which were brighter than 20.3 mag and displayed no significant variability ($J < 0.75$). In the case of a few outer fields with lower stellar density, we extended the range to 21 mag to increase the sample size. We carried out the photometric calibration of each of our 29 fields separately, and then compared the derived magnitudes for stars in common between adjacent fields to ensure their consistency. Figure 3 shows a comparison of our final calibrated magnitudes relative to the input Massey et al. catalog for one of the 29 fields located at an intermediate galactocentric radius. Note that this comparison includes stars that are significantly fainter than those used to derive the actual transformations, but we maintained the requirements of three-band photometry, variability index $J < 0.75$, and photometric uncertainties below 0.05 mag. The median differences are -0.015 ± 0.043, -0.016 ± 0.033, and -0.010 ± 0.039 mag in the B, V, and I bands, respectively. The median differences are slightly larger for more heavily crowded fields and even smaller in the outermost regions of the disk.

4. COLOR–MAGNITUDE DIAGRAMS AND CEPHEID PERIOD–LUMINOSITY RELATIONS

Figure 4 shows CMDs of ∼793,000 stars detected in the WIYN-only master frames. They are very similar to those presented by Massey et al. (2006), though our photometry is slightly deeper. We can clearly see the main sequence of massive stars along $B - V = 0$ and $V - I = 0$ mag, a sequence of foreground Milky Way dwarfs to the red of the M 33 main sequence, and the red giant and asymptotic giant branches of M 33. The Cepheid variables in our "main sample" (see below) are plotted using red symbols and delineate the instability strip.

Figure 5 shows PL relations for 705 variables that were adequately fit by a Cepheid template light curve (Section 3.2), regardless of their magnitude. The top three panels depict the BVI relations, uncorrected for extinction, while the bottom panel shows the dust-free or "Wesenheit" relation for those objects which had V and I photometry. The Wesenheit magnitude was calculated assuming a standard Cardelli et al. (1989) extinction law (see also Schlegel et al. 1998) as $W_{VI} = (2.375 \times I) - (1.375 \times V)$.

The relations presented in Figure 5 contain obvious outliers. We visually examined each individual light curve and we inspected the corresponding master image at the location of every variable. We rejected 38 objects which exhibited poorly sampled and/or extremely noisy light curves, which raised doubts about the reliability of the period determination or the nature of the stellar variability. These rejected objects are plotted using "x" symbols. We identified additional outliers in the Wesenheit PL relation, using as fiducial the corresponding OGLE-II LMC PL relation (Udalski et al. 1999). Forty-six objects lying 2.5σ or more below the mean are plotted using open triangles; they are likely to be blended Cepheids (at shorter periods) or population II Cepheids (at longer periods). Fifty-seven variables lying 3σ or more above the mean are plotted using open circles; they are likely to be blended Cepheids. We rejected outliers at different significance above and below the mean to preserve overtone Cepheids in the main sample, which consists of 564 variables plotted using filled symbols.

The top three panels of Figure 5 also show fits to the cleaned BVI main sample, keeping the slopes fixed to the values derived using the OGLE-II LMC Cepheid sample (Udalski et al. 1999).

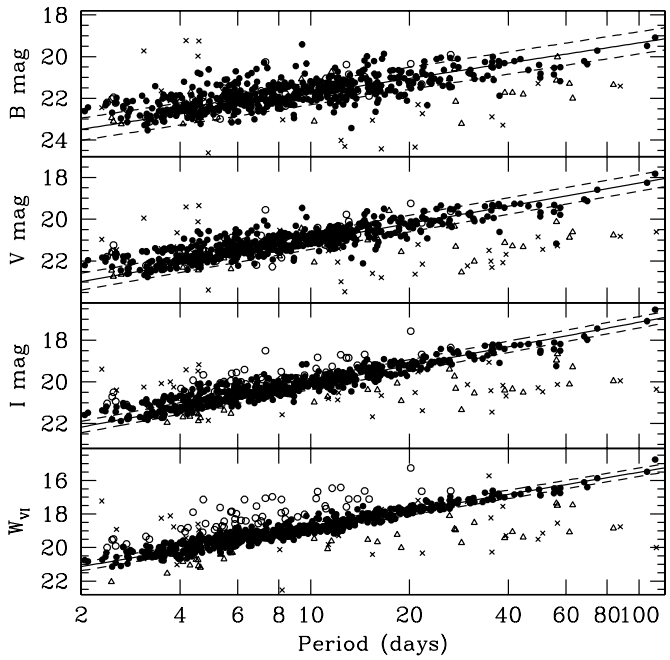

Figure 5. PL relations for M 33 Cepheids. The *B*-band, *V*-band, and *I*-band PL relations (top three panels) are uncorrected for extinction. The bottom panel is the Wesenheit (i.e., dust-free) PL relation, and based on the extinction law of Cardelli et al. (1989). All PL relations have been corrected for crowding (see Section 5). Full circles: main Cepheid sample. Open circles: abnormally bright variables, likely to be blended Cepheids. Open triangles: abnormally faint variables, likely to be blended Cepheids or population II variables. Crosses: variables with very sparse or extremely noisy light curves. Solid lines: best fit to the main Cepheid sample with periods above 8 days, keeping the slopes fixed to the values derived from the OGLE-II LMC sample (Udalski et al. 1999). Dashed lines: 2σ deviation from the fit.

Table 2
Preliminary PL-Relation Fitting Parameters

Band	Distance Modulus[a] (All Cepheids)	Distance Modulus[b] (Cleaned Sample)	Slopes[c]
B	25.39 ± 0.03	25.35 ± 0.02	−2.439
V	25.32 ± 0.03	25.26 ± 0.02	−2.779
I	25.05 ± 0.03	25.00 ± 0.03	−2.979
W_{VI}	24.77 ± 0.04	24.76 ± 0.02	−3.309

Notes. The fits were performed for Cepheids with periods longer than 8 days assuming an LMC distance modulus of 18.5 mag.
[a] Distance moduli, in magnitudes, include all Cepheids from Tables 3 to 5.
[b] Distance moduli, in magnitudes, include only the cleaned Cepheid sample as reported in Table 3.
[c] The slope values are those derived for the LMC by OGLE-II (Udalski et al. 1999).

To prevent contamination from overtones, we restricted the fit to Cepheids with $P > 8$ days. The results from the fits are given in Table 2, which are still preliminary values. We defer the determination of a new Cepheid distance to M 33 to a forthcoming publication (A. Pellerin & L. M. Macri 2011, in preparation). That publication will combine our ground-based measurements and *HST* photometry (J. Chavez et al. 2011, in preparation). Our preliminary distance moduli presented in Table 2 have only been corrected for crowding effects (see Section 5) and are consistent with previous results (Macri 2001; Freedman et al. 2001; Scowcroft et al. 2009).

Table 3 lists the coordinates, magnitudes, pulsation amplitudes, and other information for the main sample. Tables 4–6 contain the different samples of rejected outliers.

5. CROWDING CORRECTIONS

Despite the fact that our WIYN images provide a very good spatial resolution of ∼3.25 pc (0.″75 FWHM at a distance of 890 kpc), we cannot neglect the effects of crowding and blending in our photometry. Crowding can be defined as the partial overlap of two or more stellar profiles which can still be spatially resolved into individual PSFs. Blending is the more severe case where the stars are separated by less than 0.375 FWHM (following the criterion used in ALLSTAR) and cannot be spatially resolved, resulting in their detection as a single PSF. The crowding level is high in M 33, especially in the central region and in the young stellar population regions where Cepheids are often found. Furthermore, it is impossible to eliminate random projection effects within the galactic disk or binary systems. For these reasons, we need to quantitatively characterize the effects of both blending and crowding, ideally in a separate way. A detailed study of these effects in M 31 and M 33 was carried out by Mochejska et al. (2000, 2001c) and we followed their approach as discussed below.

In this publication, we address crowding corrections, which can be derived via artificial star simulations and applied to our entire Cepheid sample. Corrections for blends cannot be applied statistically, since they require individual imaging of every variable at higher angular resolution. Fortunately, the disk of M 33 has been extensively covered by the *HST*, which has a diffraction-limited spatial resolution ∼10× better than our WIYN images. A companion paper (J. Chavez et al. 2011, in preparation) presents PSF photometry of all available *HST* images that overlap with our Cepheid sample. In the absence of higher-resolution images, blends can sometimes be identified via abnormal light curve amplitude ratios or colors. We will explore the effectiveness of these cuts in a forthcoming publication (A. Pellerin & L. M. Macri 2011, in preparation).

We derived the crowding corrections using images of M 33 obtained with the Advanced Camera for Surveys (ACS) on board *HST*. We used the Multimission Archive at STScI[6] (MAST) to select observations obtained in the F475W, F606W, and F814W filters (equivalent to *B*, *V*, and *I*, respectively) which had significant overlap with our fields. The raw images were pipeline-processed by MAST. We further processed the reduced images using the PyRAF/STSDAS[7] MultiDrizzle task (Fruchter et al. 2009) to correct for optical distortion, remove cosmic rays, and combine multiple images of the same field. We carried out PSF photometry using DAOPHOT and ALLSTAR as previously described in Section 3.1. We verified that the photometry was consistent with the work of Williams et al. (2009). More details on the *HST* photometry will be presented by J. Chavez et al. (2011, in preparation).

Since we wanted to characterize the effect of crowding in our WIYN frames in a manner that was decoupled from the effects of blending, we started by identifying stars in the *HST* photometry which had no detectable neighbors within a radius of 0.″38. This is equivalent to the half-width at half-maximum of the PSF in the WIYN master frames. Next, we simulated a WIYN master frame using the DAOPHOT task ADDSTAR, placing all stars detected in the *HST* photometry at suitably rescaled CCD coordinates and with the proper instrumental magnitudes, using the ground-based PSF derived in 3.1. Lastly, we added a sky background with the same mean and standard deviation

[6] http://archive.stsci.edu
[7] PyRAF and STSDAS are products of the Space Telescope Science Institute, which is operated by AURA for NASA.

Table 3
M 33 Cepheids—Main Sample (Abridged)

Designation [M33SSS]	R.A.	Decl.	Period	V^a	I	B	σV	σI	σB	Amp V	Amp I	Amp B	C_V	C_I	C_B	Data Set
J013425.57+310029.2	23.60654	31.00812	2.052	22.202	21.590	22.613	0.002	0.006	0.011	0.085	0.054	0.119	0.183	0.158	0.088	WD
J013319.01+302512.3	23.32920	30.42008	2.096	21.963	21.484	22.438	0.007	0.037	0.033	0.103	0.100	0.183	0.173	0.154	0.080	WO
J013438.46+310155.9	23.66026	31.03220	2.319	21.835	21.370	99.999	0.001	0.004	9.999	0.151	0.147	0.121	0.167	0.149	9.999	WD
J013256.63+301849.8	23.23594	30.31382	2.370	22.024	21.405	22.340	0.013	0.043	0.033	0.496	0.313	0.718	0.176	0.150	0.077	WO
J013258.16+302505.2	23.24235	30.41810	2.387	21.830	21.191	22.230	0.014	0.030	0.043	0.186	0.148	0.238	0.167	0.142	0.072	WO
J013243.21+302653.2	23.18006	30.44811	2.483	22.274	21.799	22.684	0.017	0.125	0.053	0.389	0.252	0.533	0.187	0.167	0.091	WO
J013349.33+310219.8	23.45556	31.03884	2.548	21.826	21.441	22.214	0.001	0.007	0.012	0.086	0.054	0.122	0.167	0.152	0.072	DO
J013330.16+303417.7	23.37568	30.57158	2.560	21.662	21.200	21.974	0.009	0.040	0.026	0.152	0.169	0.185	0.160	0.142	0.063	WO
J013454.32+305929.4	23.72635	30.99150	2.640	22.448	21.880	22.966	0.025	0.023	0.100	0.439	0.311	0.684	0.195	0.170	0.103	WO
J013324.20+302248.9	23.35084	30.38026	2.686	21.779	21.013	22.375	0.008	0.023	0.028	0.175	0.081	0.220	0.165	0.135	0.078	WO
J013332.36+302819.8	23.38483	30.47216	2.689	22.004	21.152	22.472	0.006	0.044	0.042	0.333	0.081	0.339	0.175	0.140	0.082	WO
J013447.66+305805.7	23.69860	30.96824	2.748	21.778	21.127	22.123	0.006	0.026	0.016	0.245	0.190	0.346	0.165	0.139	0.068	WO
J013221.78+302059.5	23.09077	30.34985	2.765	22.610	21.733	23.139	0.029	0.035	0.096	0.404	0.262	0.641	0.202	0.164	0.111	WO
J013421.36+305806.2	23.58901	30.96839	2.769	22.377	21.785	22.860	0.013	0.055	0.044	0.450	0.322	0.633	0.191	0.166	0.098	WO
J013335.18+305425.0	23.39660	30.90694	2.773	21.750	21.188	22.181	0.016	0.042	0.064	0.115	0.076	0.161	0.164	0.142	0.070	WO

Notes.
[a] The mean magnitudes are in the Vega system and corrected for crowding, with crowding values reported in the three columns C_V, C_I, and C_B.

(This table is available in its entirety in a machine-readable form in the online journal. A portion is shown here for guidance regarding its form and content.)

Table 4
Abnormally Faint/Likely Type II Cepheids (Abridged)

Designation [M33SSS]	R.A.	Decl.	Period	V^a	I	B	σV	σI	σB	Amp V	Amp I	Amp B	C_V	C_I	C_B	Data Set
J013353.74+305848.6	23.47390	30.98017	2.472	21.607	21.794	99.999	0.021	0.040	9.999	0.490	0.302	9.999	0.158	0.167	9.999	WO
J013229.99+303141.9	23.12494	30.52830	2.477	22.454	99.999	22.939	0.008	9.999	0.036	0.441	9.999	0.531	0.195	9.999	0.102	WO
J013328.84+301942.6	23.37015	30.32849	2.508	22.740	99.999	23.104	0.031	9.999	0.102	0.500	9.999	0.720	0.208	9.999	0.109	WO
J013232.55+302534.5	23.13562	30.42626	2.649	22.646	99.999	23.238	0.020	9.999	0.088	0.510	9.999	0.729	0.204	9.999	0.116	WO
J013244.23+303936.4	23.18431	30.66011	3.179	22.134	99.999	22.856	0.007	9.999	0.018	0.461	9.999	0.688	0.180	9.999	0.098	WO
J013417.35+304505.4	23.57228	30.75151	3.655	22.254	21.956	22.619	0.001	0.011	0.008	0.414	0.055	0.625	0.186	0.174	0.088	WD
J013308.61+302503.5	23.28586	30.41764	4.085	22.309	21.693	23.234	0.011	0.042	0.026	0.402	0.271	0.573	0.188	0.162	0.115	WO
J013452.65+305836.7	23.71936	30.97685	4.290	22.103	21.664	22.738	0.018	0.108	0.074	0.514	0.323	0.760	0.179	0.161	0.093	WO
J013353.38+304743.1	23.47240	30.79531	4.312	21.325	99.999	21.702	0.003	9.999	0.007	0.239	9.999	0.329	0.146	9.999	0.053	WO
J013326.22+303219.1	23.35926	30.53865	4.391	21.714	99.999	22.393	0.000	9.999	0.004	0.223	9.999	0.283	0.162	9.999	0.079	WD
J013330.48+304417.6	23.37698	30.73823	4.474	22.043	21.491	22.713	0.019	0.072	0.051	0.368	0.247	0.495	0.176	0.154	0.092	WO
J013355.92+304720.2	23.48300	30.78893	4.541	22.146	21.554	23.014	0.030	0.041	0.111	0.497	0.316	0.720	0.181	0.156	0.105	WO
J013320.35+304539.3	23.33478	30.76092	4.550	22.440	21.878	23.064	0.021	0.060	0.080	0.311	0.172	0.223	0.194	0.170	0.107	WO
J013415.34+305523.5	23.56392	30.92320	4.617	22.132	21.735	22.936	0.029	0.071	0.096	0.432	0.270	0.690	0.180	0.164	0.102	WO
J013301.76+302607.4	23.25732	30.43540	5.317	21.725	21.169	22.189	0.025	0.039	0.089	0.319	0.198	0.483	0.163	0.141	0.071	WD

Notes.
[a] The mean magnitudes are in the Vega system and corrected for crowding, with crowding values reported in the three columns C_V, C_I, and C_B.

(This table is available in its entirety in a machine-readable form in the online journal. A portion is shown here for guidance regarding its form and content.)

as the actual WIYN master frame we were simulating. We visually inspected the simulated images to ensure they were comparable to the actual master frames. Given the smaller field of view of ACS relative to WIYN, there were relatively few isolated stars at the brightest magnitude levels. In order to obtain better statistics, we randomly removed faint isolated stars in the *HST* photometry and replaced them with bright ones. We generated several simulated images with these artificial bright stars to allow statistically meaningful results without increasing the crowding level of the images.

Once the simulated images were generated, we carried out PSF photometry in the same manner as we had done on the actual master images. We then compared the recovered and input magnitudes of the unblended stars identified in the first step. The results of this exercise are presented in Figure 6, separately for each band. We found that the crowding bias increases for fainter stars, reaching ∼0.2 mag at the faint end. We fit a second-order polynomial to the results and corrected our photometry accordingly. We conducted these simulations and measurements using all the available ACS fields which overlapped with our Cepheids, to probe regions of different surface brightness, ranging from 20 to 23 mag arcsec^{-2}. We found no statistically significant trend as a function of surface brightness.

6. CATALOG OF M 33 CEPHEIDS

Tables 3–5 present the coordinates and photometric properties of Cepheid variables discovered in this survey, separated into three categories: main sample, abnormally faint/likely population II variables, and abnormally bright/likely blended Cepheids. Only a few lines of each catalog are presented in the printed version; the complete catalogs are available in the electronic edition of the journal and in the project Web site[8]. Column 1 contains the designation of each variable following the IAU standard; we have selected the acronym "M33SSS" for our project. Celestial coordinates (J2000.0 R.A. and decl.) are

[8] http://faculty.physics.tamu.edu/lmacri/M33SSS/index.html

Table 5
Abnormally Bright/Likely Blended Cepheids (Abridged)

Designation [M33SSS]	R.A.	Decl.	Period	V[a]	I	B	σV	σI	σB	Amp V	Amp I	Amp B	C_V	C_I	C_B	Data Set
J013325.08+305807.6	23.35448	30.96879	2.398	21.795	21.040	22.205	0.001	0.005	0.009	0.158	0.063	0.252	0.166	0.136	0.071	DO
J013319.28+304831.5	23.33033	30.80876	2.485	21.563	20.710	22.025	0.007	0.025	0.031	0.085	0.055	0.127	0.156	0.123	0.065	WO
J013444.34+305217.2	23.68477	30.87145	2.508	21.239	20.501	21.953	0.044	0.025	0.042	0.475	0.417	0.315	0.143	0.116	0.062	WO
J013354.21+305859.4	23.47588	30.98318	2.548	21.687	20.936	22.230	0.013	0.027	0.052	0.129	0.089	0.148	0.161	0.132	0.072	WO
J013446.14+304928.2	23.69226	30.82451	2.749	22.034	21.089	22.511	0.026	0.032	0.075	0.343	0.216	0.493	0.176	0.138	0.083	WD
J013440.10+305905.7	23.66709	30.98492	3.149	22.216	21.006	22.929	0.009	0.022	0.015	0.462	0.179	0.899	0.184	0.135	0.101	WO
J013243.67+302610.2	23.18197	30.43618	3.225	22.365	21.160	23.137	0.001	0.024	0.009	0.372	0.177	0.476	0.191	0.141	0.111	WD
J013310.12+303355.3	23.29215	30.56535	4.027	21.361	20.317	22.164	0.018	0.021	0.084	0.343	0.205	0.673	0.148	0.109	0.070	WO
J013451.98+304318.3	23.71660	30.72175	4.144	21.502	20.475	22.245	0.010	0.019	0.029	0.104	0.119	0.193	0.153	0.115	0.073	WO
J013339.32+304725.2	23.41382	30.79033	4.228	22.090	20.709	22.789	0.021	0.024	0.079	0.346	0.217	0.517	0.178	0.123	0.095	WO
J013351.94+304658.8	23.46640	30.78299	4.384	21.393	19.922	22.075	0.008	0.012	0.018	0.487	0.322	0.738	0.149	0.096	0.066	WO
J013306.29+303050.3	23.27619	30.51396	4.689	21.428	20.444	21.957	0.000	0.002	0.005	0.131	0.053	0.202	0.150	0.114	0.062	DO
J013406.94+304258.0	23.52893	30.71611	4.711	21.496	19.662	22.166	0.009	0.012	0.031	0.271	0.136	0.296	0.153	0.088	0.070	WO
J013359.39+304213.8	23.49744	30.70384	4.782	21.521	20.277	22.469	0.005	0.009	0.037	0.496	0.303	0.749	0.154	0.108	0.082	WO
J013400.30+304808.0	23.50127	30.80223	5.101	21.592	20.472	22.371	0.003	0.006	0.018	0.429	0.268	0.644	0.157	0.115	0.078	WO

Notes.
[a] The mean magnitudes are in the Vega system and corrected for crowding, with crowding values reported in the three columns C_V, C_I, and C_B.

(This table is available in its entirety in a machine-readable form in the online journal. A portion is shown here for guidance regarding its form and content.)

Table 6
Rejected Variables

Designation [M33SSS]	R.A.	Decl.	Period[a]	V[a, b]	I[a, b]	B[a]	σV	σI	σB	Amp V	Amp I	Amp B	C_V	C_I	C_B	Data Set
J013308.82+304608.7	23.28673	30.76907	2.310	20.964	19.390	22.448	0.008	0.006	0.016	0.086	0.067	0.344	0.132	0.079	0.081	WD
J013300.57+304255.9	23.25239	30.71554	2.563	21.466	20.394	99.999	0.060	0.025	9.999	0.210	0.079	9.999	0.152	0.112	9.999	WO
J013426.55+304334.6	23.61061	30.72628	3.105	19.946	20.250	19.729	0.007	0.016	0.059	0.118	0.076	0.167	0.096	0.107	0.005	WO
J013412.00+304020.0	23.55002	30.67222	3.509	21.411	20.080	21.641	0.012	0.019	0.033	0.148	0.067	0.238	0.150	0.101	0.051	WO
J013413.38+303618.0	23.55575	30.60501	3.738	21.369	19.998	22.108	0.015	0.010	0.043	0.131	0.082	0.239	0.148	0.098	0.068	WO
J013351.26+304504.5	23.46360	30.75126	3.824	21.326	20.250	21.920	0.007	0.007	0.023	0.144	0.126	0.221	0.146	0.107	0.061	WO
J013354.37+310101.3	23.47655	31.01702	3.918	20.648	20.805	99.999	0.011	0.022	9.999	0.099	0.067	9.999	0.120	0.127	9.999	WO
J013251.03+303535.1	23.21263	30.59309	4.173	19.413	19.418	19.232	0.007	0.020	0.020	0.226	0.211	0.207	0.079	0.080	0.000	WO
J013401.43+304631.8	23.50596	30.77551	4.537	20.122	19.484	19.980	0.009	0.009	0.008	0.111	0.071	0.162	0.102	0.082	0.009	WO
J013336.91+303020.1	23.40378	30.50558	4.564	19.348	19.177	19.250	0.005	0.006	0.013	0.121	0.058	0.110	0.077	0.073	0.000	WO
J013223.81+303023.9	23.09922	30.50664	4.880	23.389	21.845	24.615	0.034	0.106	0.226	0.481	0.289	0.733	0.240	0.169	0.189	WO
J013303.85+302120.3	23.26603	30.35565	8.050	20.531	20.359	99.999	0.001	0.003	9.999	0.147	0.164	9.999	0.116	0.111	9.999	WD
J013228.14+303414.0	23.11724	30.57056	8.183	20.880	21.577	99.999	0.018	0.040	9.999	0.288	0.179	9.999	0.129	0.157	9.999	WD
J013327.04+304209.7	23.36266	30.70270	8.217	21.199	99.999	23.032	0.001	9.999	0.012	0.211	9.999	0.111	0.141	9.999	0.106	WD
J013319.91+302018.6	23.33297	30.33851	11.325	21.516	20.801	21.885	0.008	0.018	0.031	0.202	0.074	0.284	0.154	0.127	0.060	WO
J013427.14+303452.0	23.61309	30.58112	12.080	22.051	20.864	99.999	0.035	0.064	9.999	0.573	0.185	9.999	0.177	0.129	9.999	WO
J013425.66+303538.5	23.60692	30.59404	12.168	21.412	20.520	99.999	0.061	0.037	9.999	0.402	0.219	9.999	0.150	0.116	9.999	WO
J013424.59+303448.1	23.60246	30.58002	12.369	22.990	99.999	24.017	0.015	9.999	0.009	0.261	9.999	0.531	0.220	9.999	0.155	WD
J013257.31+304317.6	23.23878	30.72156	12.701	23.472	99.999	24.304	0.106	9.999	0.134	0.637	9.999	0.574	0.245	9.999	0.171	WO
J013218.18+304039.1	23.07577	30.67754	15.420	22.595	21.675	23.052	0.002	0.008	0.011	0.434	0.195	0.671	0.201	0.162	0.107	DO
J013433.08+303524.2	23.63785	30.59006	16.413	22.793	20.656	24.424	0.026	0.016	0.045	0.651	0.564	0.665	0.211	0.121	0.178	WD
J013319.46+304546.7	23.33110	30.76296	20.810	22.629	20.512	24.343	0.035	0.022	0.155	0.532	0.307	0.811	0.203	0.116	0.173	WO
J013420.25+305049.7	23.58438	30.84715	21.240	21.210	19.517	22.300	0.003	0.007	0.020	0.416	0.403	0.696	0.142	0.083	0.075	WD
J013306.75+304938.4	23.27814	30.82732	21.886	22.146	21.381	22.733	0.188	0.109	0.283	0.723	0.244	0.816	0.181	0.149	0.093	WO
J013420.18+305132.1	23.58409	30.85891	30.044	22.231	20.134	99.999	0.031	0.019	9.999	0.839	0.406	9.999	0.185	0.103	9.999	WO
J013454.42+305122.9	23.72677	30.85635	34.925	21.494	19.066	99.999	0.016	0.010	9.999	0.444	0.295	9.999	0.153	0.070	9.999	WO
J013454.89+305421.5	23.72869	30.90598	35.400	22.011	20.421	99.999	0.004	0.003	9.999	0.557	0.369	0.545	0.175	0.113	9.999	WD
J013251.87+305003.1	23.21611	30.83418	35.666	22.306	21.449	22.891	0.212	0.083	0.264	0.605	0.323	0.755	0.188	0.152	0.100	WO
J013321.54+304445.6	23.33974	30.74599	38.500	22.081	20.172	23.287	0.035	0.011	0.078	0.689	0.495	0.317	0.178	0.104	0.118	WO
J013435.99+304656.4	23.64997	30.78234	39.351	21.683	20.673	99.999	0.044	0.010	9.999	0.462	0.328	9.999	0.161	0.122	9.999	WO
J013308.88+302402.4	23.28699	30.40068	49.303	20.844	20.282	21.290	0.012	0.022	0.045	0.453	0.408	0.591	0.127	0.108	0.040	WO
J013255.21+304802.6	23.23005	30.80072	50.915	21.445	20.477	99.999	0.079	0.052	9.999	0.522	0.395	9.999	0.151	0.115	9.999	WO
J013251.24+304939.8	23.21350	30.82772	56.467	21.272	20.124	99.999	0.020	0.011	9.999	0.417	0.232	9.999	0.144	0.103	9.999	WD
J013322.15+302114.2	23.34230	30.35395	87.691	20.816	19.951	21.415	0.000	0.002	0.004	0.229	0.163	0.388	0.126	0.097	0.044	DO
J013412.45+303350.2	23.55186	30.56394	113.000	20.608	20.353	99.999	0.032	0.024	9.999	0.474	0.310	9.999	0.119	0.111	9.999	WO

Notes.
[a] Periods and magnitude values are subject to changes, since their light curves have not been well defined.
[b] All magnitudes are in the Vega system and corrected for crowding, with crowding values reported in the three columns C_V, C_I, and C_B.

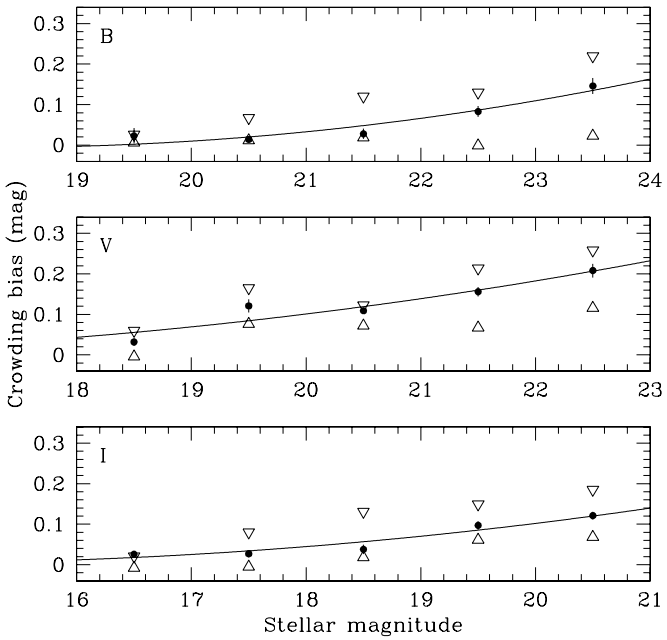

Figure 6. Crowding bias as a function of magnitude, derived using stars known to be free of blends through higher-resolution *HST* imaging. The filled symbols indicate the median value of each magnitude bin, while the triangular symbols indicate the 25% and 75% quartile ranges. The solid lines indicate the second-order polynomial fit that was used to correct all our photometry for crowding.

provided in decimal degrees in Columns 2 and 3. The period of variability (in days) is reported in Column 4. Given the exceptionally long time coverage of our survey, we were able to derive periods with very high precision. The mean magnitudes in the *V*, *I*, and *B* bands already corrected for crowding bias are listed in Columns 5, 6, and 7, respectively. The 1σ uncertainties on the mean magnitudes are provided in Columns 8, 9, and 10 for the *V*, *I*, and *B* bands, respectively. The best-fit light curve amplitude in *V*, *I*, and *B* are given in Columns 11, 12, and 13, respectively. The crowding corrections already applied to the mean magnitudes are reported in Columns 14, 15, and 16 for *V*, *I* and *B*, respectively. The last column indicates the data set on which the photometric values are based, i.e., "WIYN+DIRECT" (WD), "WIYN-only" (WO), or "DIRECT-only" (DO) photometry, as discussed in Section 3.1. Since the variability search was conducted in the *V* band (Section 3.2), where the largest number of images was obtained, all variables in this catalog have *V*-band properties but some of the fainter variables may lack *B* or *I* data.

Examples of Cepheid light curves covering the entire range of periods are plotted in Figure 7, along with their best-fit templates. All light curve data are available to the community at the Web site previously mentioned, or by contacting the authors.

We compared our Cepheid catalog with the variable-star catalog of Hartman et al. (2006). Five hundred forty-four of our variables were located within 5″ of a variable star in that catalog, while 123 had no entries. We also compared the periods found for Cepheids in common between both catalogs, using periods kindly provided by J. Marquette et al. (2010, private communication). The vast majority of the periods were in excellent agreement, with a mean difference of 0.05%.

7. CONCLUSION

We have presented the details and first results of a long-term synoptic *BVI* survey of the stellar content of M 33. We have carried out time-series PSF photometry of ∼793,000 stars with

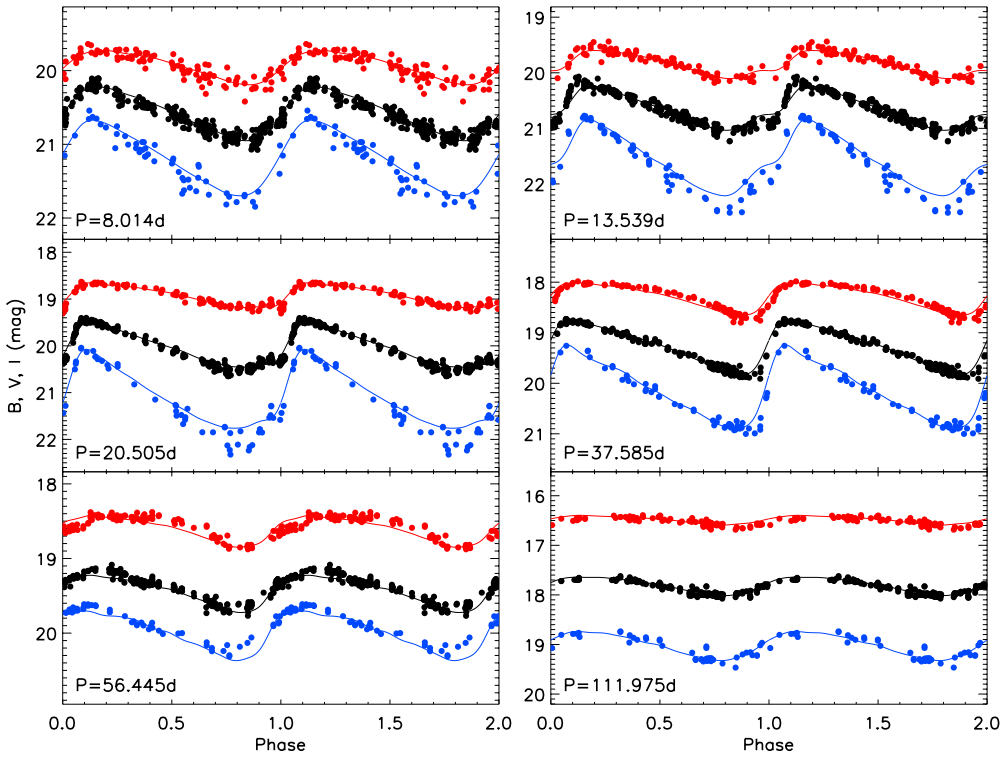

Figure 7. Examples of light curves of M 33 Cepheids. The three *B*-band (blue), *V*-band (black), and *I*-band (red) light curves are shown. The points represent the photometric observations, while the lines are the best-fit templates from Yoachim et al. (2009). The periods, in days, are indicated within each panel. The Cepheids shown here are J013314.77+303907.2, J013305.58+303825.2, J013324.63+303517.8, J013252.21+303715.1, J013254.34+303805.4, and J013253.81+303525.3, in order of increasing period.

(A color version of this figure is available in the online journal.)

$V < 25$ mag and have identified 667 variables whose light curves are consistent with Cepheid pulsation. After rejecting abnormally faint and bright objects, we obtain a main sample of 564 Cepheid variables, which represents an increase of a factor of two relative to the DIRECT project sample of Macri et al. (2001b). We present catalogs which include the periods, mean magnitudes, and light curve amplitudes for each object. Light curve data will be made available online.

We carried out detailed simulations based on archival *HST* images to quantify biases in our photometry due to crowding effects. A companion paper (J. Chavez et al. 2011, in preparation) will quantify the level of blending for a sub-sample of our Cepheids, using *HST* data. A detailed analysis of the effects of blending and crowding on the derivation of a Cepheid distance to M 33 will be presented by A. Pellerin & L. M. Macri (2011, in preparation).

L.M.M. acknowledges initial support for this project by NASA through Hubble Fellowship grant HST-HF-01153 from the Space Telescope Science Institute and by the National Science Foundation through a Goldberg Fellowship from the National Optical Astronomy Observatory. We acknowledge financial support from a Texas A&M University faculty startup fund. We thank P. Yoachim for generating *B*-band Cepheid light curve templates. This research has made use of NASA's Astrophysics Data System.

REFERENCES

Bonanos, A. Z., et al. 2006, ApJ, 652, 313
Bresolin, F. 2011, ApJ, in press (arXiv:1102.0044)
Bresolin, F., Pietrzyński, G., Gieren, W., & Kudritzki, R. 2005, ApJ, 634, 1020
Bresolin, F., Stasińska, G., Vílchez, J. M., Simon, J. D., & Rosolowsky, E. 2010, MNRAS, 404, 1679
Cardelli, J. A., Clayton, G. C., & Mathis, J. S. 1989, ApJ, 345, 245
Freedman, W. L., et al. 2001, ApJ, 553, 47
Fruchter, A., et al. 2009, The MultiDrizzle Handbook, Version 3.0 (3rd ed.; Baltimore, MD: STScI)
Hartman, J. D., Bersier, D., Stanek, K. Z., Beaulieu, J., Kaluzny, J., Marquette, J., Stetson, P. B., & Schwarzenberg-Czerny, A. 2006, MNRAS, 371, 1405
Högbom, J. A. 1974, A&AS, 15, 417
Hubble, E. P. 1925, ApJ, 62, 409
Hubble, E. P. 1926, ApJ, 63, 236
Komatsu, E., et al. 2011, ApJS, 192, 18
Leavitt, H. S., & Pickering, E. C. 1912, Harv. Coll. Obs. Circ., 173, 1
Macri, L. M. 2001, PhD thesis, Harvard Univ.
Macri, L. M., Stanek, K. Z., Sasselov, D. D., Krockenberger, M., & Kaluzny, J. 2001a, AJ, 121, 870
Macri, L. M., Stanek, K. Z., Sasselov, D. D., Krockenberger, M., & Kaluzny, J. 2001b, AJ, 121, 861
Magrini, L., Vílchez, J. M., Mampaso, A., Corradi, R. L. M., & Leisy, P. 2007, A&A, 470, 865
Massey, P., Olsen, K. A. G., Hodge, P. W., Strong, S. B., Jacoby, G. H., Schlingman, W., & Smith, R. C. 2006, AJ, 131, 2478
Mochejska, B. J., Kaluzny, J., Stanek, K. Z., Sasselov, D. D., & Szentgyorgyi, A. H. 2001a, AJ, 121, 2032
Mochejska, B. J., Kaluzny, J., Stanek, K. Z., Sasselov, D. D., & Szentgyorgyi, A. H. 2001b, AJ, 122, 2477
Mochejska, B. J., Kaluzny, J., Stanek, K. Z., Sasselov, D. D., & Szentgyorgyi, A. H. 2001c, arXiv:astro-ph/0103440
Mochejska, B. J., Macri, L. M., Sasselov, D. D., & Stanek, K. Z. 2000, AJ, 120, 810
Riess, A. G., et al. 2009, ApJ, 699, 539
Roberts, D. H., Lehar, J., & Dreher, J. W. 1987, AJ, 93, 968
Sandage, A., Tammann, G. A., Saha, A., Reindl, B., Macchetto, F. D., & Panagia, N. 2006, ApJ, 653, 843
Schlegel, D. J., Finkbeiner, D. P., & Davis, M. 1998, ApJ, 500, 525
Scowcroft, V., Bersier, D., Mould, J. R., & Wood, P. R. 2009, MNRAS, 396, 1287
Stanek, K. Z., Kaluzny, J., Krockenberger, M., Sasselov, D. D., Tonry, J. L., & Mateo, M. 1998, AJ, 115, 1894
Stetson, P. B. 1987, PASP, 99, 191
Stetson, P. B. 1994, PASP, 106, 250
Stetson, P. B. 1996, PASP, 108, 851
Udalski, A., Szymanski, M., Kubiak, M., Pietrzynski, G., Soszynski, I., Wozniak, P., & Zebrun, K. 1999, Acta Astron., 49, 201
Williams, B. F., Dalcanton, J. J., Dolphin, A. E., Holtzman, J., & Sarajedini, A. 2009, ApJ, 695, L15
Yoachim, P., McCommas, L. P., Dalcanton, J. J., & Williams, B. F. 2009, AJ, 137, 4697
Zaritsky, D., Kennicutt, R. C., Jr., & Huchra, J. P. 1994, ApJ, 420, 87